HHS Public Access

Author manuscript

*J Interdiscip Histopathol*. Author manuscript; available in PMC 2016 December 01.

Published in final edited form as:

*J Interdiscip Histopathol*. 2016 ; 4(2): 29–33. doi:10.5455/jihp.20160623053540.

# Characterization of the blood brain barrier in pediatric central nervous system neoplasms

**Christopher S. Hong**[1,2], **Winson Ho**[1], **Martin G. Piazza**[1,3], **Abhik Ray-Chaudhury**[1], **Zhengping Zhuang**[1], and **John D. Heiss**[1]

[1]Department of Surgical Neurology Branch, National Institutes of Health, Bethesda, MD 20892, USA

[2]Department of Neurosurgery, Yale University School of Medicine, New Haven, CT, 06510, USA

[3]Department of Neurosurgery, University of North Carolina, Chapel Hill, NC, 27599, USA.

## Abstract

**Objective—**The normal blood–brain barrier (BBB) is composed of tight junctions between endothelial cells and surrounding astrocyte foot processes. Breakdown of the physiological astrocyte-endothelial cell relationship occurs in adult metastatic and primary brain tumors. However, the astrocyte-endothelial cell relationship has not been studied in pediatric tumors.

**Materials and Methods—**Utilizing specimens from cases of pilocytic astrocytoma (n = 5), medulloblastoma (n = 5), and low-grade diffuse astrocytoma (n = 1), immunofluorescence were performed using primary antibodies against CD31, glial fibrillary acidic protein (GFAP), and aquaporin 4 (AQ4). Clinical, magnetic resonance imaging, operative, and histopathological findings were analyzed.

**Results—**Strongly-enhancing areas of medulloblastoma exhibited complete BBB breakdown with sparse GFAP and AQ4 staining around CD31-positive vessels. Moderately enhancing regions of pilocytic astrocytomas exhibited regions of intact BBB and vasculature surrounded by dense GFAP staining but reduced and disorganized AQ4 staining, suggesting tumor cells could not fulfill physiological BBB support. Non-enhancing low-grade diffuse astrocytoma demonstrated intact BBB with intense peri-microvasculature GFAP and AQ4 staining. AQ4 stained so strongly that AQ4 visualization alone delineated CD31-positive vessels.

**Conclusion—**Taken together, BBB breakdown in pediatric tumors corresponds to a loss of normal endothelial cell-astrocyte foot process relationships. Further development of pharmaceutical agents capitalizing on this disrupted BBB is warranted in medulloblastoma and pilocytic astrocytoma. However, BBB integrity remains a challenge in treating low-grade diffuse astrocytoma before progression toward secondary glioblastoma.



Address for correspondence: Zhengping Zhuang, 10 Center Drive, Building 10, Room 03D05, Bethesda, MD 20892, USA. Phone: 301-435- 8445, Fax: 301-402-0536, zhuangp@ninds.nih.gov.

The authors declare no conflicts of interest.

**Keywords**

Blood–brain barrier; glioma; medulloblastoma; pediatric brain tumor; pilocytic astrocytoma

## INTRODUCTION

Primary neoplasms of the central nervous system (CNS) are the most common solid tumors in the pediatric population [1]. While aggressive surgical resection and adjuvant radiotherapy have proven to be efficacious for long-term disease control, this approach is often contraindicated due to tumor location and risk of neurocognitive toxicity. As such, there is intense ongoing research to develop medical therapies that may act in concert with maximally tolerable surgery and radiation to accomplish complete tumor eradication.

It is well-known that the blood–brain barrier (BBB) presents a significant challenge to successful delivery of therapeutic drugs to the CNS. The normal BBB is comprised tight junctions between capillary endothelial cells, which form a cohesive basement membrane that is further reinforced by an organized sheath of perivascular astrocyte foot processes [2]. It is well recognized that certain pediatric CNS neoplasms exhibit characteristic BBB breakdown, evidenced by contrast enhancement on magnetic resonance imaging (MRI). Among this group of tumors are medulloblastoma and pilocytic astrocytoma, two primary brain tumors found predominantly in the pediatric population and at opposite ends of the World Health Organization grading spectrum. While complete surgical resection confers a positive prognosis in both cases, a gross total resection is often not accomplished due to the propensity for these tumors to develop in and around the brainstem near eloquent structures [3,4]. As such, further characterization of the BBB in these tumors is warranted to better design the delivery of novel therapeutic agents that can infiltrate the tumor parenchyma, eradicate residual tumor, and obviate excessively aggressive surgical and radiation management.

Previously, our group reported a correlation between MRI enhancement in adult metastatic and primary CNS tumors and breakdown of the normal astrocyte-endothelial cell relationship of the BBB on immunofluorescence [5]. Using tumor samples from pediatric patients with MRI-enhancing medulloblastoma and pilocytic astrocytoma as well as non-enhancing low-grade diffuse astrocytoma, we explored whether similar disruptions in the physiological astrocyte-endothelial cell relationship explained the radiographic evidence of BBB breakdown in these pediatric CNS tumors.

## MATERIALS AND METHODS

### Patients and Tumors

Tumors were collected and analyzed under an institutional review board-approved protocol (NIH 03-N-0164). All patients provided informed consent for study participation. Additional formalin-fixed paraffin-embedded tissues of medulloblastoma and pilocytic astrocytoma samples were obtained, anonymously, under a materials transfer agreement from an outside institution.

### Imaging Evaluation

The patients underwent pre-operative T1-weighted MRI before and after administration of gadolinium contrast agent. Lesions were deemed to be contrast enhancing or non-enhancing based on hyperintensity on post-contrast T1-weighted MRI. T2-weighted images were used for determining tumor distribution of non-enhancing lesions.

### Histological Analysis

Hemotoxylin and eosin (H and E) staining was performed on all tissue specimens to confirm pathological diagnosis as well as distinguish morphological features of tumor vasculature and surrounding perivascular cellular architecture.

### Immunofluorescence Analysis

Immunofluorescence staining was performed for each tumor specimen using antibodies against CD31 (anti-mouse, 1:200) (Millipore, Billerica, MA), glial fibrillary acidic protein (GFAP) (anti-rabbit, 1:1000) (Abcam, Cambridge, UK), and aquaporin 4 (AQ4) (anti-rabbit, 1:200) (Millipore). AQ4 is a marker of astrocytic foot processes and has been previously used as a reliable measure of astrocyte-endothelial cell relationship integrity [6,7]. Double immunofluorescence staining was performed for CD31 and GFAP; and CD31 and AQ4, using a protocol described previously [5]. The following secondary antibodies were used at 1:1000 dilution:donkey serum anti-mouse IgG absorbing at a wavelength of 568 nm (Life Technologies, Carlsbad, CA) and donkey serum anti-rabbit IgG absorbing at a wavelength of 488 nm (Life Technologies). Immunofluorescent images were captured at ×40 magnification using a Leica (Wetzlar, Germany) LSM 510 confocal microscope, while H and E images were obtained at ×40 magnification using a Nikon (Tokyo, Japan) Eclipse Ci microscope with a Nikon DS-Fi2 camera.

## RESULTS

### Medulloblastoma

A representative T1-weighted MRI of a medulloblastoma is shown [Figure 1], demonstrating a heterogeneously enhancing large posterior fossa mass of the fourth ventricle, measuring 3.8 cm × 4.8 cm × 5.2 cm, causing mild tonsillar herniation and significant obstructive hydrocephalus. Microscopic review of the surgical specimen showed sheets of round, hyperchromatic neoplastic cells amid calcification, apoptosis, and micronecroses, consistent with medulloblastoma [Figure 2a]. In addition, there were areas of focal positivity for synaptophysin and GFAP. On immunofluorescence, there was virtually absent staining of GFAP [Figure 2b] and AQ4 [Figure 2c] staining around CD31 positive vessels. Similar findings were present for the other cases of medulloblastoma.

### Pilocytic Astrocytoma

A representative T1-weighted MRI of a pilocytic astrocytoma is shown in Figure 3, exhibiting a heterogeneously enhancing mass with mixed solid and cystic components in the posterior fossa. The enhancing portion measured 5.3 cm × 3.8 cm × 4.4 cm. The histopathological review revealed a highly cellular tumor against a background of mucinous

material, abundant Rosenthal fibers, occasional eosinophilic granular bodies, and hyalinized blood vessels, characteristic of pilocytic astrocytoma [Figure 4a]. Immunostaining demonstrated diffuse positivity for GFAP and negativity for mutated p53. On immunofluorescent analysis, abundant GFAP signal was evident, consistent with an astrocyte tumor cell lineage [Figure 4b]. However, staining of AQ4 was reduced and disorganized [Figure 4c], suggesting tumor cells could not fulfill their physiological role of supporting the BBB. Histology and immunofluorescence of the other specimens of pilocytic astrocytoma demonstrated similar findings.

### Low Grade Diffuse Astrocytoma

A brain MRI demonstrates a representative case of low-grade diffuse astrocytoma [Figure 5], evidenced by a 3.9 cm × 1.9 cm × 4.0 cm non-enhancing infiltrative lesion within the medial right frontal lobe with significant fluid-attenuated inversion recovery edema. Histopathological review of the surgical specimen exhibited mild hypercellularity with atypical cells, a low proliferation index, and absence of vascular proliferation or necrosis, consistent with low-grade diffuse astrocytoma [Figure 6a]. Immunohistochemical staining was positive for IDH1 and p53 mutations. Additional molecular studies were negative for 1p/19q co-deletion or BRAF mutations. Immunofluorescent staining demonstrated an intact BBB with intense GFAP [Figure 6b] and AQ4 [Figure 6c] signal around the microvasculature. Notably, AQ4 stained so strongly that visualization of AQ4 alone accurately delineated the outline of CD31 positive vessels.

## DISCUSSION

In this study, we found that the enhancement seen on MRI of pilocytic astrocytomas and medulloblastomas correlates with loss of the normal astrocyte-endothelial cell relationship of intratumoral vasculature. We have previously reported these findings in adult primary and metastatic cerebral neoplasms [5] and have re-iterated our methods and results in a pediatric population.

Pilocytic astrocytomas exhibit a characteristic radiologic appearance of a well-circumscribed round or oval mass, hypo- to isointense on T1-weighted images and markedly enhancing after contrast administration [8-10]. On a histological level, BBB breakdown has been attributed to chronic glomeruloid degenerative hyalinization as well as presumably tumor cell-induced microvascular proliferation. Our data demonstrated a stark contrast between GFAP abundance and AQ4 scarcity, suggesting disruption of the normal endothelial cell-astrocyte relationship.

Similar to pilocytic astrocytomas, medulloblastomas demonstrate heterogeneous enhancement on MRI, presumably due to leaky glomeruloid vessels characteristically seen on histopathology [11,12]. Numerous studies have shown that these tumors exhibit potent angiogenesis and that the density of blood vessels inversely correlates with patient survival [13,14]. In each of our five samples, there was scarce GFAP staining, indicative of a virtual absence of astrocytes in the tumor parenchyma. Medulloblastomas are thought to originate from a primitive neuroectodermal cell with partial neuronal differentiation, as evidenced by frequent positive staining for synaptophysin and NeuN [13,14]. Some tumors exhibit focal

areas of glial differentiation, but our results showed that GFAP-positive staining cells did not fulfill the normal endothelial cell support role. Unlike astrocytomas, the inability of normal astrocytes to populate the densely cellular tumor parenchyma of medulloblastomas causes BBB breakdown.

Consistent with previous findings [5], the low-grade diffuse astrocytoma in our study exhibited organized and tight perivascular associations between GFAP and AQ4 staining of astrocytic foot processes and CD31-positive endothelial cells. On the H and E stain, there was little evidence of microvascular proliferation, suggesting the absence of significant angiogenesis in these tumors. It has been previously suggested that infiltrating tumor cells of low-grade diffuse astrocytomas feed off of diffusing nutrients from existing, phenotypically normal vasculature [15]. Our results confirmed that the astrocyte-endothelial cell relationship in the blood vessels of low-grade diffuse astrocytomas remains intact.

In summary, this study found a loss of the normal tight association between perivascular astrocyte foot processes and endothelial cells, contributing to BBB breakdown in pilocytic astrocytomas and medulloblastomas. Despite increased permeability of the BBB, curative chemotherapeutic treatment of these tumors remains a challenge [16-18]. This may be due to a lack of tumor dependence upon leaky neovascularization with preferential feeding from normal brain vasculature [19]. As our data show, diffuse low-grade diffuse astrocytomas exhibit an intact BBB, which likely contributes significantly to the poor overall survival response of these tumors to systemic chemotherapies [20,21]. Further studies may clarify to what degree tumor cells are supplied by neovasculature with disrupted perivascular tight junctions and whether this feature can be capitalized on for development of novel therapeutics. This is of particular importance for the pediatric population where radiotherapy carries a significant risk of long-term neurocognitive effects and where deep tumor location often precludes complete surgical resection.

## ACKNOWLEDGMENTS

The authors thank Christopher Pierson, M.D., Ph.D., for kindly providing additional tissue samples for analysis in this study. This work was supported by the Intramural Research Program at the National Institutes of Health (NIH), National Cancer Institute, and the NIH Medical Research Scholars Program, a public-private partnership supported jointly by the NIH and generous contributions to the Foundation for the NIH through Pfizer, Inc., The Doris Duke Charitable Foundation, The Alexandria Real Estate Equities, Inc. and Mr. and Mrs. Joel S. Marcus, and the Howard Hughes Medical Institute, as well as other private donors. For a complete list, please visit the Foundation website at: http://fnih.org/work/education-training-0/medical-research-scholars-program.

## REFERENCES

1. Babcock MA, Kostova FV, Guha A, Packer RJ, Pollack IF, Maria BL. Tumors of the central nervous system: Clinical aspects, molecular mechanisms, unanswered questions, and future research directions. J Child Neurol. 2008; 23:1103–21. [PubMed: 18952577]
2. Rubin LL, Barbu K, Bard F, Cannon C, Hall DE, Horner H, et al. Differentiation of brain endothelial cells in cell culture. Ann N Y Acad Sci. 1991; 633:420–5. [PubMed: 1665033]
3. Cyrine S, Sonia Z, Mounir T, Badderedine S, Kalthoum T, Hedi K, et al. Pilocytic astrocytoma: A retrospective study of 32 cases. Clin Neurol Neurosurg. 2013; 115:1220–5. [PubMed: 23265563]
4. Akay KM, Izci Y, Baysefer A, Atabey C, Kismet E, Timurkaynak E. Surgical outcomes of cerebellar tumors in children. Pediatr Neurosurg. 2004; 40:220–5. [PubMed: 15687736]

5. Nduom EK, Yang C, Merrill MJ, Zhuang Z, Lonser RR. Characterization of the blood-brain barrier of metastatic and primary malignant neoplasms. J Neurosurg. 2013; 119:427–33. [PubMed: 23621605]
6. Gundersen GA, Vindedal GF, Skare O, Nagelhus EA. Evidence that pericytes regulate aquaporin-4 polarization in mouse cortical astrocytes. Brain Struct Funct. 2014; 219:2181–6. [PubMed: 23982198]
7. Roales-Buján R, Páez P, Guerra M, Rodríguez S, Vío K, Ho-Plagaro A, et al. Astrocytes acquire morphological and functional characteristics of ependymal cells following disruption of ependyma in hydrocephalus. Acta Neuropathol. 2012; 124:531–46. [PubMed: 22576081]
8. Lee YY, Van Tassel P, Bruner JM, Moser RP, Share JC. Juvenile pilocytic astrocytomas: CT and MR characteristics. AJR Am J Roentgenol. 1989; 152:1263–70. [PubMed: 2718863]
9. Coakley KJ, Huston J 3rd, Scheithauer BW, Forbes G, Kelly PJ. Pilocytic astrocytomas: Well-demarcated magnetic resonance appearance despite frequent infiltration histologically. Mayo Clin Proc. 1995; 70:747–51. [PubMed: 7630212]
10. Palma L, Guidetti B. Cystic pilocytic astrocytomas of the cerebral hemispheres. Surgical experience with 51 cases and long-term results. J Neurosurg. 1985; 62:811–5. [PubMed: 3998829]
11. Fruehwald-Pallamar J, Puchner SB, Rossi A, Garre ML, Cama A, Koelblinger C, et al. Magnetic resonance imaging spectrum of medulloblastoma. Neuroradiology. 2011; 53:387–96. [PubMed: 21279509]
12. Yeom KW, Mobley BC, Lober RM, Andre JB, Partap S, Vogel H, et al. Distinctive MRI features of pediatric medulloblastoma subtypes. AJR Am J Roentgenol. 2013; 200:895–903. [PubMed: 23521467]
13. Moschovi M, Koultouki E, Stefanaki K, Sfakianos G, Tourkantoni N, Prodromou N, et al. Prognostic significance of angiogenesis in relation to Ki-67, p-53, p-27, and bcl-2 expression in embryonal tumors. Pediatr Neurosurg. 2011; 47:241–7. [PubMed: 22309998]
14. MacDonald TJ, Taga T, Shimada H, Tabrizi P, Zlokovic BV, Cheresh DA, et al. Preferential susceptibility of brain tumors to the antiangiogenic effects of an alpha(v) integrin antagonist. Neurosurgery. 2001; 48:151–7. [PubMed: 11152340]
15. Claes A, Idema AJ, Wesseling P. Diffuse glioma growth: A guerilla war. Acta Neuropathol. 2007; 114:443–58. [PubMed: 17805551]
16. Karajannis MA, Legault G, Fisher MJ, Milla SS, Cohen KJ, Wisoff JH, et al. Phase II study of sorafenib in children with recurrent or progressive low-grade astrocytomas. Neuro Oncol. 2014; 16:1408–16. [PubMed: 24803676]
17. Gururangan S, Chi SN, Young Poussaint T, Onar-Thomas A, Gilbertson RJ, Vajapeyam S, et al. Lack of efficacy of bevacizumab plus irinotecan in children with recurrent malignant glioma and diffuse brainstem glioma: A pediatric brain tumor consortium study. J Clin Oncol. 2010; 28:3069–75. [PubMed: 20479404]
18. Terashima K, Chow K, Jones J, Ahern C, Jo E, Ellezam B, et al. Long-term outcome of centrally located low-grade glioma in children. Cancer. 2013; 119:2630–8. [PubMed: 23625612]
19. Doolittle ND, Muldoon LL, Culp AY, Neuwelt EA. Delivery of chemotherapeutics across the blood-brain barrier: Challenges and advances. Adv Pharmacol. 2014; 71:203–43. [PubMed: 25307218]
20. Gilbert MR, Wang M, Aldape KD, Stupp R, Hegi ME, Jaeckle KA, et al. Dose-dense temozolomide for newly diagnosed glioblastoma: A randomized phase III clinical trial. J Clin Oncol. 2013; 31:4085–91. [PubMed: 24101040]
21. Shaw EG, Wang M, Coons SW, Brachman DG, Buckner JC, Stelzer KJ, et al. Randomized trial of radiation therapy plus procarbazine, lomustine, and vincristine chemotherapy for supratentorial adult low-grade glioma: Initial results of RTOG 9802. J Clini Oncol. 2012; 30:3065–70.

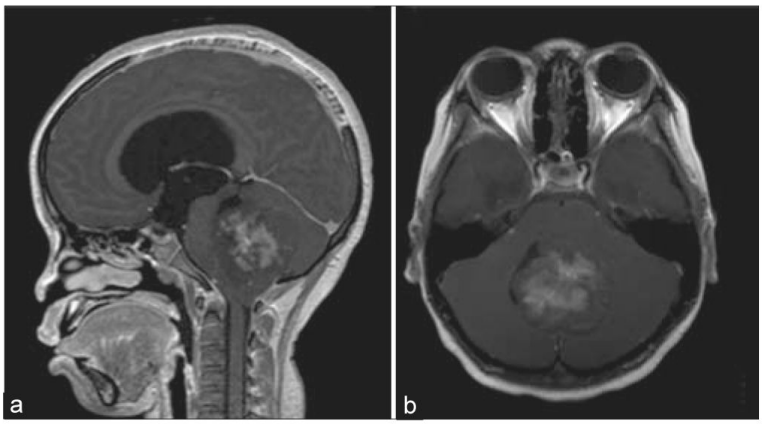


**Figure 1.**

Radiographic characteristics of medulloblastoma. (a) Sagittal and (b) axial views of a T1-weighted magnetic resonance imaging after contrast administration demonstrating a heterogeneously enhancing mass located in the fourth ventricle

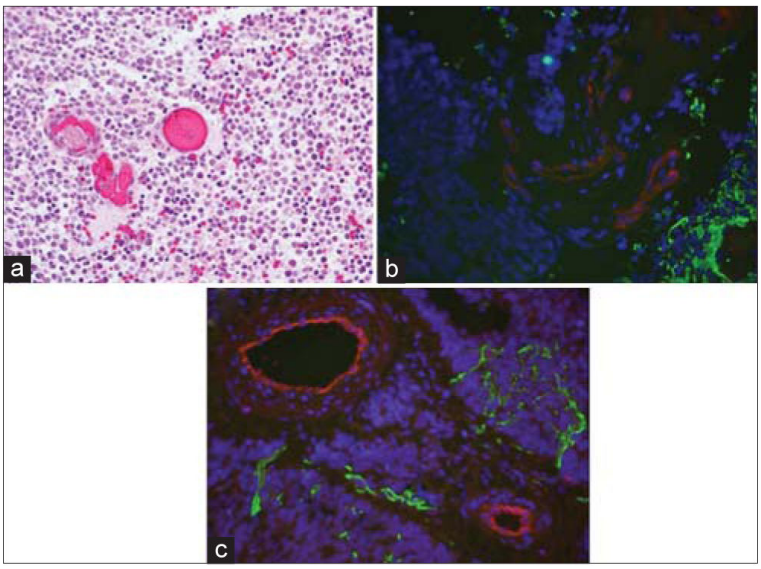


**Figure 2.**

Histopathological review of medullloblastoma. (a) An H and E stain, ×400 of the specimen showing hypercellular, undifferentiated small round blue cells, amid apoptosis and micronecrosis, consistent with medulloblastoma. (b) Specimen stained for glial fibrillary acidic protein (green) showing virtual absence of astrocytes within tumor mass (DAPI; blue) and endothelial cells (red) denude of normal, perivascular astrocytic foot processes. (c) Specimen stained for aquaporin 4 (green) similarly showing disruption of normal endothelial cell (red)-astrocyte relationship

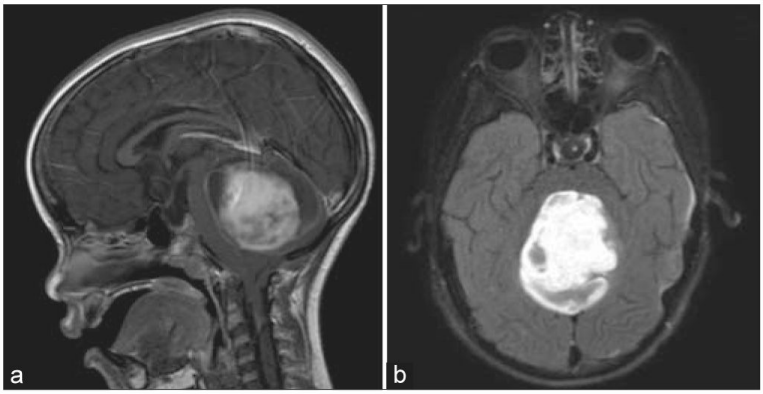


**Figure 3.**

Radiographic characteristics of pilocytic astrocyma. (a) Sagittal and (b) axial views of a T1-weighted magnetic resonance imaging after contrast administration demonstrating an enhancing mass within the cerebellum

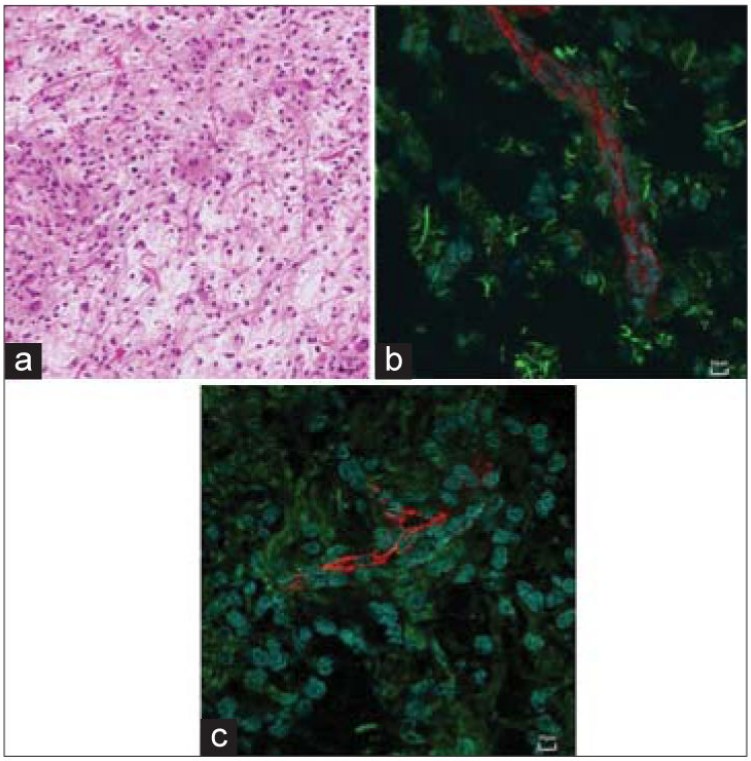


**Figure 4.**

Histopathological review of pilocytic astrocytoma. (a) An H and E stain, 400× of the specimen showing hypercellularity with rosenthal fibers, microvascular proliferation, and eosinophilic granular bodies, consistent with pilocytic astrocytoma. (b) Specimen stained for glial fibrillary acidic protein (green) showing abundance of astrocytes, albeit disorganized near endothelial cells (red). (c) Specimen stained for aquaporin 4 (green) showing significant loss of perivascular astrocyte foot processes suggestive of blood brain barrier breakdown

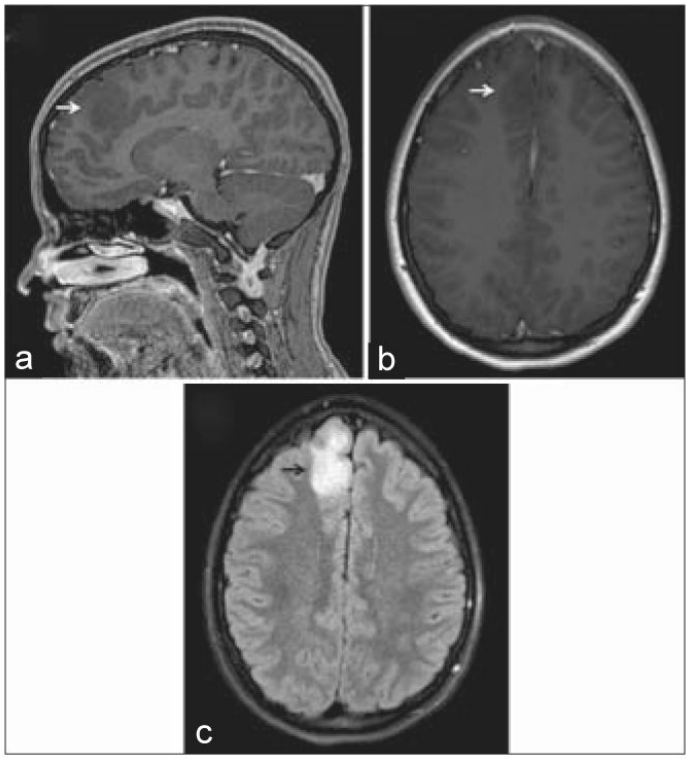


**Figure 5.**
Radiographic characteristics of diffuse astrocytoma. (a) Sagittal and (b) axial views of a T1-weighted magnetic resonance imaging (MRI) after contrast administration, demonstrating a non-enhancing hypointense mass (white arrows) abutting the falx. (c) On a T2-weighted MRI, there was significant associated fluid-attenuated inversion recovery edema (black arrow)

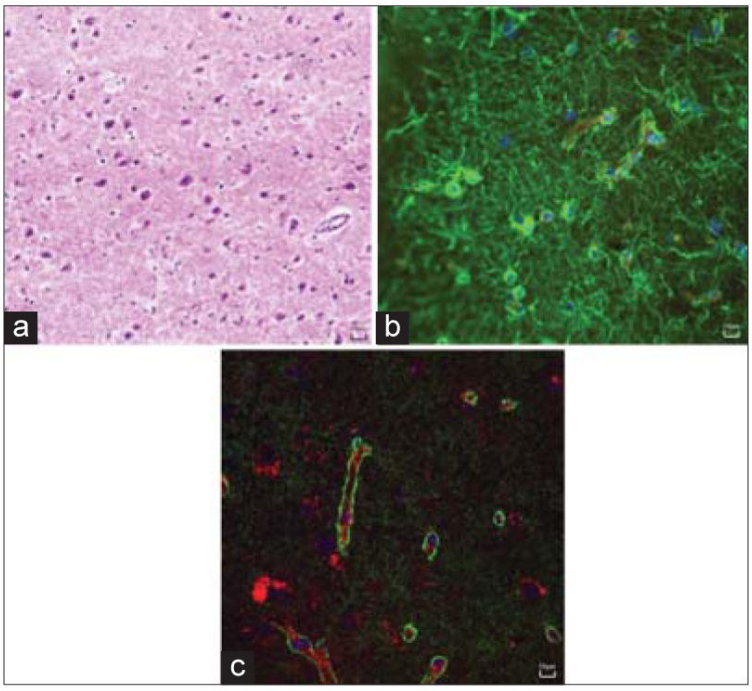


**Figure 6.**

Histopathological review of low-grade diffuse astrocytoma. (a) An H and E stain, ×400 of the specimen showing low to moderate cellularity with increased mitotic figures but absence of microvascular proliferation and necrosis. (b) Specimen stained for glial fibrillary acidic protein (green) showing abundance of astrocytes, both in perivascular space near CD31 (red)-positive blood vessels and in tumor parenchyma. (c) Specimen stained for aquaporin 4 (green) showing tight organization around blood vessels (red), illustrating preserved integrity of the blood–brain barrier